# A Monolayer Dually Polarized High-Order Space Harmonic Leaky-Wave SIW Antennas With Fixed and Scanning Beam Capability

**MOHAMMAD REZA RAHIMI (Student Member, IEEE),**
**MOHAMMAD S. SHARAWI (Senior Member, IEEE), AND KE WU (Fellow, IEEE)**

Poly-Grames Research Center, Polytechnique Montreal, Montreal, QC H3T 1J4, Canada

CORRESPONDING AUTHOR: M. R. RAHIMI (e-mail: mohammad-reza.rahimi@polymtl.ca)

**ABSTRACT** In this work, the concept of high-order space harmonics (HSHs) applied to a hybrid form of nonradiative dielectric (NRD) waveguide and substrate-integrated square waveguide (SIW) involving both $TE_{10}$ and $TE_{01}$ modes is investigated with aim to develop multi-functional dually polarized leaky-wave antennas (DP-LWAs). A polarization-selective coupling (PSC) mechanism is used to guide the two orthogonally oriented modes in the hybrid structure to achieve a polarization diversity feature. The polarization effect on unit-cell geometrical structures is examined for different characteristics of LWA such as propagation constant behavior, leakage ratio, and scanning range variation. In addition, we demonstrate how the extrinsic characteristics of HSHs in a one-dimensional periodic LWA and its unit-cell analysis can provide design flexibility through two case studies. In the first case of demonstration, we show a dually polarized multi-beam LWA design with wide scanning capability in which we use both even and odd HSHs of n $\epsilon$ [$-1$, $-2$]). The second antenna design case is concerned with a DP-LWA having the capability of fixed and scanning beams operation by using a combinatory set of PSC and four HSHs of n $\epsilon$ [$-1$, $-2$, $-3$, $-4$]. Two DP-LWA prototypes are demonstrated as proofs of concept, and the obtained experimental results show a very good agreement with their simulation and analysis counterparts.

**INDEX TERMS** One-dimensional periodic leaky-wave antenna (1D-periodic LWA), higher-order space harmonics (HSHs), polarization-selective coupler (PSC), nonradiative dielectric (NRD) waveguide, substrate integrated waveguide (SIW), dually polarized antenna (DPA).

## I. INTRODUCTION

ONE-DIMENSIONAL periodic leaky-wave antennas (1D-periodic LWAs) have some distinguishable features such as low profile, single layer, wide bandwidth, and inexpensive beam steering solution compared to phased array antennas which usually require couplers, phase shifters, and complex bulky feeding or beam-forming networks [1], [2], [3]. Based on their geometrical structures, LWAs are divided into three categories: uniform [4], quasi-uniform [5], [6], and periodic [7], [8], [9], [10], [11], [12]. Regardless of this classification, most of the LWAs usually produce a narrow fan beam which finds many potential applications in frequency modulated continuous-wave (FMCW) radars [13], feeding of high gain reflector antennas [14],

sparse 3D imaging [15], multi-target sensor detection [16], and fading mitigation in multipoint communications [17].

With the recent and rapid evolutionary growth of wireless communications like 5G networks, bandwidth consumption has become a major concern for most system design engineers. Fortunately, deploying FR2 bands (24.2 to 54.6 GHz) in the millimeter-wave (30 to 300 GHz) frequency range with polarization diversity offers a potential solution to fulfill this gap. In this case, orthomode transducer (OMT) is an essential component for polarization diversity. Different methodologies can be used in designing OMTs, such as Bøifot [18], turnstile junctions [19], [20], dual-mode double ridge waveguides [21], and groove gap waveguides [22]. However, most have 3D geometrical structures which make

them hard to integrate with other parts. Planar OMT structures were investigated in [23], [24] at the expense of using multi-layers. Nevertheless, a low-profile monolayer planar OMT with integration capability should be highly attractive for 5G applications and beyond.

Additionally, considerable efforts have been made in realizing dually polarized antennas (DPAs) due to the spectrum limitation and high data demand in cellular systems. DPAs judging from their mechanisms and radiation properties are divided into two different categories. The first category belongs to the DPA with the capability of fixed beam operations [25], [26], [27], [28], [29], [30], [31], where the antenna beam of each polarization targets a similar angle. These types of DPAs are more suitable for channel capacity improvement especially in dense areas where we encounter user plane (UE) traffic [32], [33]. The second category is related to DPAs featuring a different beam direction for each polarization [34], [35]. These types of DPAs provide a wider coverage compared to the first category since the beam of each polarization targets different angles. It should be mentioned that besides this categorization, the features of beam steering and polarization diversity can also be beneficial for multi-user streaming and broadcasting where the use of a multiple input multiple output (MIMO) technology can improve the cell throughput (base station) performances [36], [37].

Several methods were proposed to realize a dually polarized LWA (DP-LWA), such as the dual-mode transmission line [38], symmetrical spoof surface plasmon polariton lines [39], back-to-back slot array [40], OMT based LWA [35], partially reflected surface (PRS) LWA [41], metamaterial LWA [42], and lens LWA [43]. However, all those methodologies can only provide a single beam operation for each polarization which makes them unsuitable for multi-beam operations, which are essential in 5G new radio (NR) [44]. A multi-beam mechanism can be used to enhance the spectral efficiency, power delay profile, reduce recovery times [45], and also to provide reduction in computational complexity and access times [46]. Furthermore, a code book technique can be applied to simultaneous multi-beam radiators to achieve faster initial access times [47]. Some methods were also used to achieve common source multi-beam LWAs, such as dual-mode transmission line [48], defected ground structure (DGS) [49] and aperture coupled feeding [50], [51]. However, applying all these methodologies [48], [49], [50], [51] to a DPA for achieving a multi-beam operation is challenging, and to the authors' best knowledge, do not yet exist in literature. In addition to multi-beam operation, dual-polarization, and beam steering features, it is also beneficial for the antenna to have a fixed beam operation, especially for point-to-point communications [52]. However, the beam in most LWAs usually steers with frequency which makes them unamenable for fixed beam operations. Besides, using single beam operation there will be a high possibility of link failure due to the blockage effect. This issue can be overcome by using multi-beam operation and assigning a code book to the radiated signals. In this case, if one of the beams fails then the alternative one can still provide a reliable connection [53].

In this work, we introduce a method for designing and analyzing 1D-periodic LWA as a common source dually polarized multi-beam antenna. We try to benefit from the hybrid form of the nonradiative dielectric (NRD) waveguide and the substrate-integrated square waveguide (SIW) to achieve the polarization diversity for our LWA design. The authors in [54], [55] demonstrated a planar OMT which has the potential integration capacity with antenna. However, they did not investigate this feature in their work since the focus was on developing the concept and theory of OMT operation. Hence, in this work, we demonstrate a comprehensive analysis in this regard; we analyze the behavior of two OMT modes ($TE_{10}$ and $TE_{01}$), along with an LWA, for different higher-order space harmonic (HSH) of each OMT operation mode. This work differs from [56] where the authors discussed the HSH behavior for a single polarization LWA and their focus was on the broadside condition of $n = -2$ space harmonic. Here, however, we tackle the HSH behavior with the presence of two orthogonal modes in which the geometrical effect of the LWA's unit cell on the propagation constant, leakage ratio, and stop-band for single and dual-mode operations is investigated and their differences are highlighted. Furthermore, the design flexibility in terms of multi-beam alignment of the HSH for two OMT modes is also investigated.

In the first design reported in this work, we demonstrate a dually polarized multi-beam steering LWA where we use a combination of one even and one odd HSH of $n \in [-1, -2]$ of each OMT mode. It should be mentioned that a combination of fixed beam operation along with beam steering can sufficiently reduce the volume and size of wireless communication systems and present an alternative solution for future broadcasting designs. This work also demonstrates a dually polarized multi-beam LWA with the capability of providing simultaneous fixed and scanning beam operation. In the second design, we use a combination of polarization-selective coupling (PSC) mechanism and four HSHs belonging to $n \in [-1, -2, -3, -4]$. This design is different compared to [57] where two reflector antennas with 180° phase shift between the reflected waves were used to achieve a single fixed-beam operation for their LWA. This contribution differs from [52] and [58] where the fixed single beam LWA (single polarization) is achieved at the expense of adding a mirror and glide-symmetric prisms to the structure. While, in this work, we achieve fixed multi-beam operation by utilizing the HSH concept along with beam scanning feature. To the best of our knowledge, this is the first time that an antenna with the capability of simultaneous fixed and scanning beams operation is proposed and demonstrated. Experimental results show a good agreement between the simulation, analysis, and measurements (CST STUDIO SUITE used in all simulations and analyses).

This work is organized as follows. Section II investigates LWA's unit-cell for two oriented modes and shows the analysis and experimental validation of a dually polarized multi-beam steering LWA. Section III gives the modeling, analysis and experimental validation of a DP-LWA with simultaneous fixed and scanning multi-beam capabilities. Finally, Section IV concludes the work and discusses future perspectives.

## II. DUALLY POLARIZED PERIODIC LWA
### A. EFFECT OF POLARIZATION ON UNIT-CELL RADIATED POWER

In this section, we study and analyze the effects of the $TE_{10}$ and $TE_{01}$ polarization diversity in connection to our antenna radiating element for a DP-LWA design based on the PSC concept. The performances of the periodic LWAs are predictable thanks to careful analysis of their unit-cell radiating element [4]. The geometrical shape of the radiating element is usually chosen based on the current distribution of the transmission line propagating mode. Most of the uni-polarized periodic LWAs operate with a single mode to prevent additional modes from any hybrid-mode coupling in their operation band [59]. However, for dual-polarization (if two modes are used for the antenna operation), it is necessary to examine the coupling effect between the two operating modes and its impact on the antenna performances. In addition, for each polarization, we also need to investigate the geometrical shape of the LWA's unit-cell to make sure we can get an acceptable radiating performance from it.

As a first step, we study and analyze the effect of the SIW-LWA unit-cell for two modes, namely $TE_{10}$ and $TE_{01}$. Here we are interested in examining the unit-cell in the Ka-band. Therefore, the square section of the SIW-LWA's unit-cell is considered to be 3mm, using an RT6002 substrate. Based on these dimensions, the cutoffs of the $TE_{10}$ and $TE_{01}$ modes are 29 GHz, and the higher mode cutoff starts from 41.2GHz. The behavior of most periodic LWAs is usually predictable thanks to a careful analysis of their Brillouin diagram, where the relation between different space harmonics can be written as $\beta_n = \beta_0 + 2n\pi/p$. In this work (DP-LWA), we want to study the behavior of the propagation constant ($\beta_0$) of the two modes $TE_{10}$ and $TE_{01}$. Here the focus is on the $n = -1$ space harmonic. By choosing the periodicity of the LWA's unit-cell as $p = 6.9$mm and the square section's length as 3mm, the contribution of the $n = -1$ space harmonic is a single fast wave ($\beta_{-1}/k_0 \leq 1$) for the frequencies above 36 GHz where the fundamental and $n = -2$ space harmonics remain as a slow wave due to the condition of $\beta_0/k_0 \leq 1$ and $\beta_{-2}/k_0 \geq 1$, respectively. Fig. 1(a) shows the Brillouin diagram analysis in this case (the propagation model is theoretically calculated). Here we achieve the same Brillouin diagram for the $TE_{10}$ and $TE_{01}$ modes because of the square section unit-cell. It should be mentioned that besides the analysis of the Brillouin diagram, it is also necessary to investigate the radiating element's effect on the performance of the LWA.
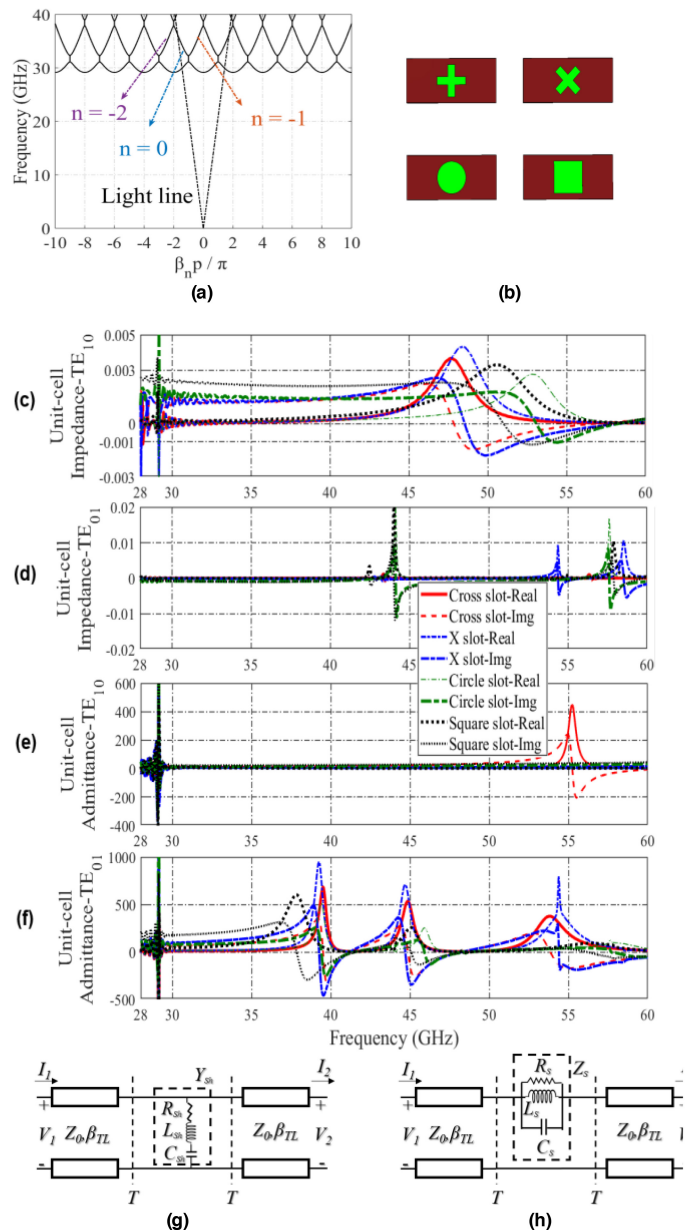


**FIGURE 1.** (a) Brillouin diagram for 1D-periodic SIW-LWA with periodicity of $p = 6.9$mm on a dielectric propagating medium of $\varepsilon_r = 2.94$ with and effective width of 3mm, (b) LWA's unit-cells, (c) radiating element impedance for $TE_{10}$ mode, (d) radiating element impedance for $TE_{01}$ mode, (e) radiating element admittance for $TE_{10}$ mode, (f) radiating element admittance for $TE_{01}$ mode, (g) equivalent circuit for $TE_{01}$, and (h) equivalent circuit for $TE_{10}$ mode.

Fig. 1(b) shows different radiating geometries that can be used for our LWA's unit-cell. Here the focus is on the upper frequency of the Ka-band, so the length of the cross-slot, X-slot, square-slot and diameter of circle-slot are considered to be $\lambda g/2$ (2.2mm) and the width of cross-slot, and X-slot are $\lambda g/10$ (0.44mm). The response of the impedance/admittance behavior of these LWA's unit-cells is demonstrated in Figs. 1(c)-(f). In this analysis, we consider modes 1 and 2 of the LWA's unit-cell as $TE_{10}$ and $TE_{01}$, respectively, where the relation for impedance

and admittance behavior based on the Z and Y matrix analysis [60] can be written as:

$$TE_{10} \rightarrow B_y = -1/Y_{2(1)1(1)} \tag{1}$$

$$TE_{01} \rightarrow B_y = -1/Y_{2(2)1(2)} \tag{2}$$

$$TE_{10} \rightarrow C_z = 1/Z_{2(1)1(1)} \tag{3}$$

$$TE_{01} \rightarrow C_z = 1/Z_{2(2)1(2)} \tag{4}$$

where By and Cz are the parameters of the ABCD matrix of the LWA's unit-cell. The analysis of Figs. 1(c)-(f) shows that the LWA's radiating elements have different responses for each polarization. For instance, comparing Figs. 1(c)-(d) indicates that we can only get the contribution of the real part of the radiating element impedance for the $TE_{10}$ mode for the frequency range of interest ($35 < f_{GHz} < 39$), while we do not have any response for the $TE_{01}$ mode over this frequency range. Besides, comparing Figs. 1(e)-(f) also shows that the contribution of the real part of the radiating element admittance only belongs to the $TE_{01}$ mode, and we have no response for the $TE_{10}$ mode in the frequency range of interest. Thus, each polarization has different circuit response. Approximate equivalent circuits for the $TE_{01}$ and $TE_{10}$ modes are illustrated in Figs. 1(g)-(h), respectively. Another point that needs to be considered here is related to the radiated power response of LWA's unit-cell. The analysis of Figs. 1(c)-(f) shows that the radiating element with a wider geometry (square-slot in this case) radiates more power compared to other LWA's unit-cells. However, the slope variation of the impedance/admittance behavior of the square-slot is sharper compared to other LWA's unit-cells in the frequency range of interest. Thus, we expect to have more gain variation for our LWA, which is not desirable. The analysis of Figs. 1(c)-(f) shows that the cross-slot can provide a suitable tradeoff between the slope variation and the real part of unit-cell's impedance/admittance behavior for both polarizations ($TE_{10}$ and $TE_{01}$ modes) within the frequency range of interest. Thus, we choose the cross slot as the radiating element for the design of the DP-LWA.

## B. EFFECT OF POLARIZATION ON UNIT-CELL PROPAGATION CONSTANT AND LEAKAGE RATIO

It should be mentioned that most of the periodic LWAs operate with a single polarization. However, adding a second polarization to the LWA will highly affect the performance of the primary one. To address this issue, we investigate the effect of single- and dual-polarization on the performance of our periodic LWA unit-cells. Figs. 2(a)-(b) show the propagation constant and leakage ratio behavior for different LWA's unit-cells for the case of single- and dual-polarization where the phase and attenuation constants can be expressed as [60]:

$$\beta = Im\left[\cosh^{-1}\left((A + D)/2\right)\right]/p \tag{5}$$

$$\alpha = Re\left[\cosh^{-1}\left((A + D)/2\right)\right]/p \tag{6}$$

Here A and D are two components of the ABCD matrix and they can be found from the Z and Y matrices. In the analysis of Figs. 2(a)-(b), we consider having transverse and longitudinal slots with single polarization and cross-slots for dual-polarization. The periodicity in the unit-cells of Fig. 2(a) is chosen based on the analysis of Fig. 1(a) and is equal to 6.9mm and the length and width of all slots are λg/2 (2.2mm) and λg/10 (0.44mm), respectively. Besides, the square section of the SIW-LWA's unit-cell is set to 3mm with the substrate RT6002. Based on these dimensions, the same cutoff is obtained for the two modes as in Section II-A. At first, we compare the operation of the $TE_{10}$ mode between the single and dual-polarization of our LWA's unit-cells. The analysis of Fig. 2(b) shows that the propagating $TE_{10}$ mode can provide a wider stop-band frequency range for the case of a single polarization (transverse slot) compared to the dual-polarization (cross-slot). In addition, the leakage ratio of propagating $TE_{10}$ mode for the case of a single polarization (transverse slot) has a higher value at the pass-band and stop-band frequencies compared to the dual-polarization (cross-slot). Hence, we should expect to have more radiated power in the single polarization (transverse slot). Furthermore, the propagation constant behavior of the propagating $TE_{10}$ mode also has different behavior for each case of the single and dual polarization at the pass-band frequency. It is expected that the propagating $TE_{10}$ mode for the dual-polarization provides more scanning range compared to the single polarization. This is attributed to the higher value and increased variation of its propagation constant ($\beta_{-1}$) (over the pass-band). On the contrary, the propagation constant behavior and leakage ratio variation of the propagating $TE_{01}$ mode has approximately similar behavior in both the single polarization (longitudinal slot) and dual-polarization (cross-slot). Hence, their radiated power and scanning angle variations must be similar. Another notable point from the analysis of Fig. 2(b) is that we also have different responses of propagating $TE_{01}$ and $TE_{10}$ modes for dual-polarization cases (cross-slot). Here the $TE_{10}$ mode can provide a wider stop-band frequency compared to the $TE_{01}$ mode scenario while the leakage ratio of these modes has an approximately similar response in their common passband frequency range. In addition, the propagation constant ($\beta_{-1}$) of the $TE_{01}$ mode shows more variation as compared to that of the $TE_{10}$ mode (in the common passband) which results in a wider scanning range and angular misalignment.

To overcome the issue of misalignment between propagation constant variations in each polarization, we investigate the geometrical effect of the cross-slot LWA's unit-cell for the two polarizations of our DP-LWA. Figs. 2(c)-(d) show the effect of slot length variation of the cross-slot for the propagating $TE_{10}$ and $TE_{01}$ modes, respectively. The periodicity of unit-cells in Figs. 2(c)-(d) is chosen based on the analysis of Fig. 1(a). The analysis of Figs. 2(c)-(d) shows that using a longer slot not only provides a wider stop band, but it also shifts down the lower edge of the stop band to lower frequencies while slightly affecting the upper stop band edge as well. In addition, using the longer slot decreases
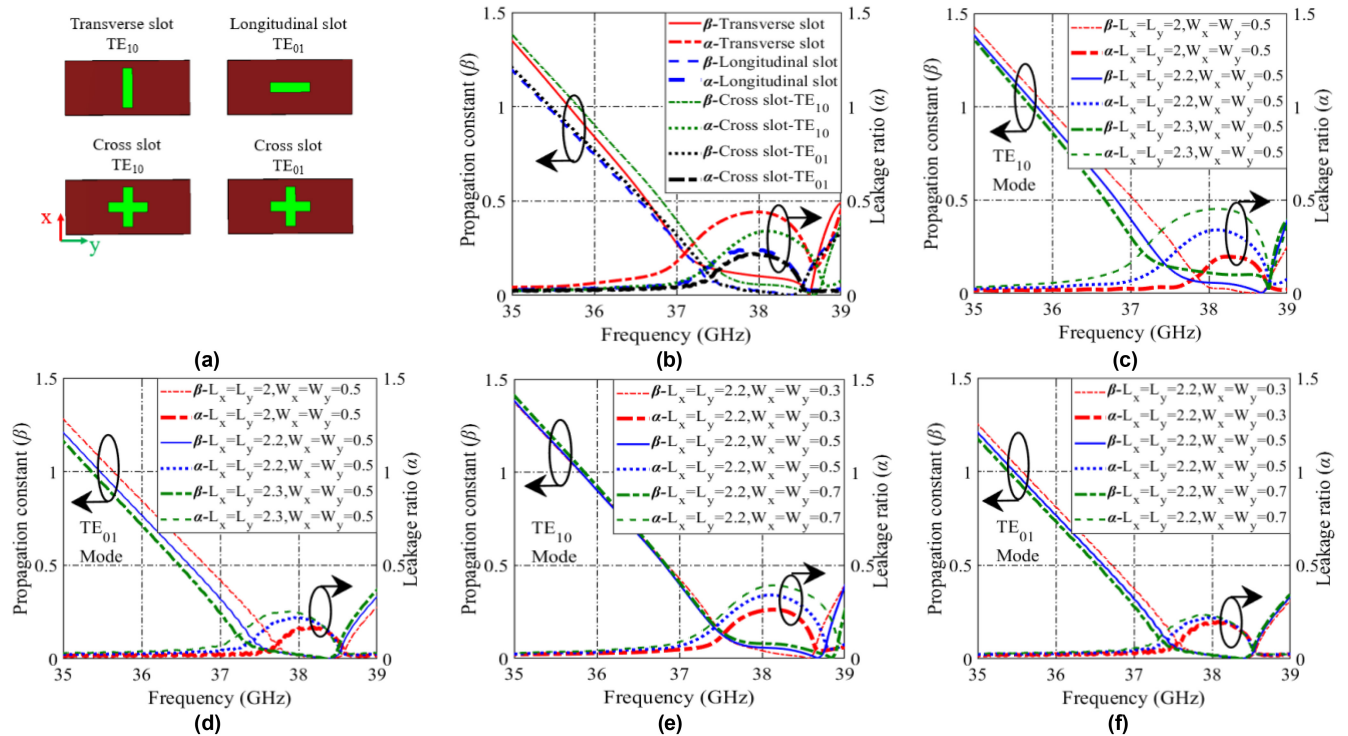
**FIGURE 2.** (a) LWA's unit-cells, (b) propagation constant and leakage ratio behavior for single and dual-polarization, (c) slot length variation effect of $TE_{10}$ mode, (d) slot length variation effect of $TE_{01}$ mode, (e) slot width variation effect of $TE_{10}$ mode, and (f) slot width variation effect of $TE_{01}$ mode.

the variation and values of the propagation constant ($\beta_{-1}$) in the passband, which results in a lower scanning range. Comparing Figs. 2(c)-(d) also shows that a propagating $TE_{10}$ mode is more sensitive to slot length variations compared to the $TE_{01}$ mode. Figs. 2(e)-(f) show the effects of slot width variations with the same condition as the length variation. The analysis of Fig. 2(e) shows that a wider slot not only provides a wider stop band, but also it shifts up the upper edge of the stop band to higher frequencies while slightly affecting the lower edge of the stop band. Also, it slightly affects the propagation constant ($\beta_{-1}$) in the passband frequency range. While for the $TE_{01}$ mode, using a wider slot decreases the variation and values of the propagation constant ($\beta_{-1}$), which results in a shorter scanning range. Besides, using a wider slot for the propagating $TE_{01}$ mode also increases the stop band and shifts down the lower edge of stop band to lower frequencies, while slightly affecting the upper edge of stop band.

The analysis of Figs. 2(c)-(f) suggests that a symmetric cross slot could provide an approximate similar response of leakage ratio for both $TE_{10}$ and $TE_{01}$ modes in the common passband frequency range. However, the propagation constant ($\beta_{-1}$) of these modes has different responses in their common passband frequency ranges. Interestingly, choosing the cross-slot as our LWA's radiating element gives us the flexibility of controlling the propagation constant for each propagating modes of the $TE_{10}$ and $TE_{01}$ since it can be approximately considered as a combination set of a transverse slot and a longitudinal slot. From the analysis

of Figs. 2(c)-(f), it is expected that an unsymmetrical cross-slot can decrease the difference between the propagation constants of each propagating mode, $TE_{10}$ and $TE_{01}$. This is shown by plotting the $\beta_{-1TE10}$ - $\beta_{-1TE01}$ of the LWA's unit-cell. In addition, if the condition of $\beta_{-1TE10} - \beta_{-1TE01} \approx 0$ is satisfied, we should expect that the phase difference between the two modes also approaches zero ($\Delta\varphi TE_{01}$ - $\Delta\varphi TE_{10} \approx 0$) and that their related beams must be in alignment. However, the $\beta_{-1TE10}$ - $\beta_{-1TE01}$ condition is only valid and applicable for the single space harmonic (this study case n = −1) operation for our DP-LWA. The beam's alignment for a dual-polarized operation (two modes operation in this study) is more complex when we are simultaneously dealing with more than one space harmonic (as fast waves) at the same frequency, since the distinction between the phase operation of each mode and their related HSH becomes more challenging and complicated.

## C. BEAM ALIGNMENT OF HSH
In order to address this issue in a comprehensive manner, first, we analyzed and studied the behavior of phase variation of different unit-cells with the capability of supporting two space harmonics as fast waves at the same frequency. Based on the analysis of $\beta_n = \beta_0 + 2n\pi/p$, we expect to get the contribution of n $\epsilon$ [−1, −2] space harmonics as fast waves by choosing the permittivity, effective width and periodicity of our SIW-LWA's unit-cell as 2.94, 3mm, and 8.5mm, respectively, in the frequency range of 35 < $f_{GHz}$ < 39. Fig. 3(a) shows its Brillouin diagram analysis,
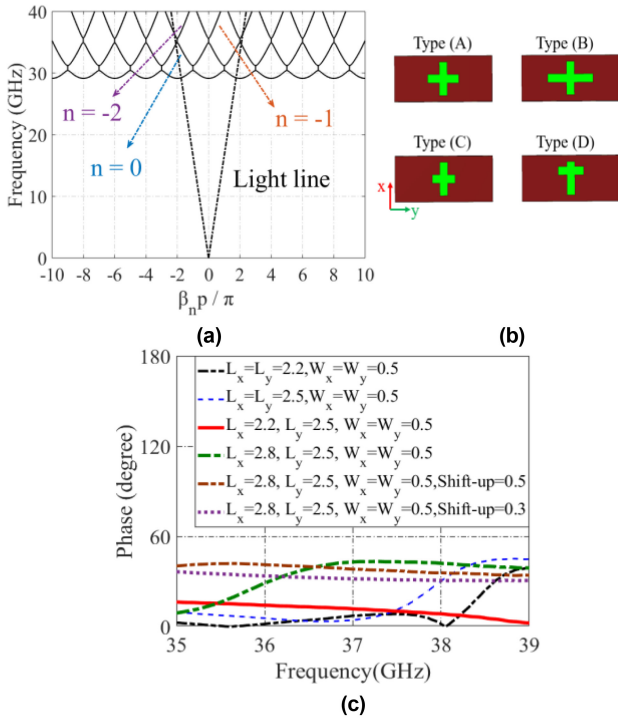
**FIGURE 3.** (a) Brillouin diagram for a 1D-periodic SIW-LWA with periodicity of *p* = 8.5mm on a dielectric propagating medium of $\varepsilon_r$ = 2.94 with and effective width of 3mm, (b) SIW-LWA's unit-cell, and (c) phase shift difference of two propagating modes of $TE_{10}$ and $TE_{01}$ for different SIW-LWA's unit-cells of Fig. 3(b).

where the n = 0 space harmonic remains as slow waves and n $\in$ [−1, −2] space harmonics behave as fast waves for frequencies above 35GHz. The Brillouin diagram of Fig. 3(a) is also applicable to both $TE_{10}$ and $TE_{01}$ modes since the SIW-LWA's unit-cell is designed to have a square section dimension (3mm). Figs. 3(b)-(c) show symmetric and asymmetric cross-slot type radiating elements with their phase shift difference response of two propagating modes of $TE_{10}$ and $TE_{01}$ ($\Delta\varphi TE_{01}$ - $\Delta\varphi TE_{10}$), respectively. In the analysis of Figs. 3(b)-(c) at first, we try to investigate the phase response behavior for two symmetric cross-slots (type A), where the length and width dimensions are set to be $\lambda$g/2 and $\lambda$g/10 for f = 35.5GHz (black line) and f = 38.5 GHz (blue line), respectively. We chose these two frequencies since they can be set as lower and upper frequencies for the passband of the Brillouin diagram of Fig. 3(a). The analysis of Fig. 3(c) shows that using a symmetric cross-slots (blue and black lines) cannot provide a flat and low response for the phase shift difference of two propagating modes ($TE_{10}$ and $TE_{01}$). However, based on the analysis of Fig. 2, we should expect to have less difference between two propagating modes' phase shift variations by using an asymmetric cross-slot in which the transverse slot has a shorter length compared to the longitudinal slot (type B). Fig. 3(c) shows that a transverse slot with dimensions of 2.2mm, and 0.5mm along with a longitudinal slot with dimensions of 2.5mm, and 0.5mm in a cross slot can provide a low value and flat response for the phase shift

difference variations between the two propagating modes (red line). Contrarily, an asymmetric cross-slot with a longer geometrical length for its transverse slot (type C) cannot provide such a flat response (green line). Besides, our analysis also shows that choosing a longer dimension for the transverse slot compared to the longitudinal slot, in addition to shifting up/down the longitudinal slot in an asymmetric cross slot (type D), not only can give us a flat response for the two propagating modes' phase shift difference but also gives us the feasibility of shifting up/down the phase shift difference between them (brown and purple lines).

Comparing the A-D responses of the radiating element in Fig. 3 indicates that a better beam alignment must be achieved for type B since it realizes a lower value of phase shift difference between the two propagating modes. It should be mentioned that the beam angle alignment between the two propagating modes in Fig. 3 does not comply with the value of the phase shift difference between the two propagating modes. This non-compliance occurs as it shows the total phase response difference between the two propagating modes and their related HSH's phases. In order to find an accurate beam angle difference between the two propagating modes and their related HSH, we investigate the behavior of the propagation constant of each mode along with the propagation constant response of each mode's HSH. Here we are interested in analyzing the unit-cells of Fig. 3 for $35 < f_{GHz} < 39$. Based on $\beta_n = \beta_0 + 2n\pi/p$, the total phase response for each propagating mode in the frequency range of our interest must be the summation of $\beta TE_{10}$ (n = −1) + $\beta TE_{10}$ (n = −2) for $TE_{10}$ mode and $\beta TE_{01}$ (n = −1) + $\beta TE_{01}$ (n = −2) for $TE_{01}$ mode. They can be written as:

$$\beta_{TE_{10}} l_z = l_z \left( \sqrt{\varepsilon_r k_0^2 - (\pi/l_x)^2} - \frac{2\pi}{p} \right)$$
$$+ l_z \left( \sqrt{\varepsilon_r k_0^2 - (\pi/l_x)^2} - \frac{4\pi}{p} \right) \quad (7)$$

$$\beta_{TE_{01}} l_z = l_z \left( \sqrt{\varepsilon_r k_0^2 - (\pi/l_y)^2} - \frac{2\pi}{p} \right)$$
$$+ l_z \left( \sqrt{\varepsilon_r k_0^2 - (\pi/l_y)^2} - \frac{4\pi}{p} \right) \quad (8)$$

where $l_z$ is the length of periodic unit-cell of our LWA. The difference between the two propagating modes is:

$$\beta_{TE_{10}} - \beta_{TE_{01}} = 2 \left( \sqrt{\varepsilon_r k_0^2 - (\pi/l_x)^2} - \sqrt{\varepsilon_r k_0^2 - (\pi/l_y)^2} \right) \quad (9)$$

It should be mentioned that the factor of 2 in (9) is only applicable when we are dealing with 2 space harmonics simultaneously (this case n $\in$ [−1, −2]). However, the conditions in (9) can also be extendable for any set combination of different space harmonics as:

$$\beta_{TE_{10}} - \beta_{TE_{01}} = m \left( \sqrt{\varepsilon_r k_0^2 - (\pi/l_x)^2} - \sqrt{\varepsilon_r k_0^2 - (\pi/l_y)^2} \right) \quad (10)$$
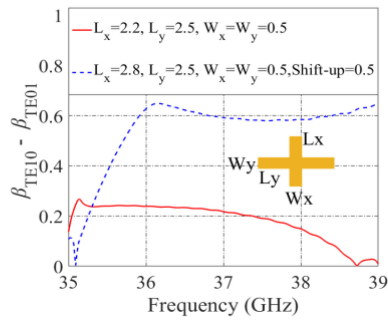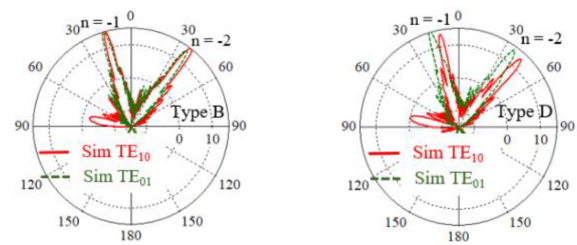
FIGURE 4. Difference between the propagation constant of $TE_{10}$ and $TE_{01}$ modes of two SIW-LWA's unit-cells of Fig. 3 (types B and D).
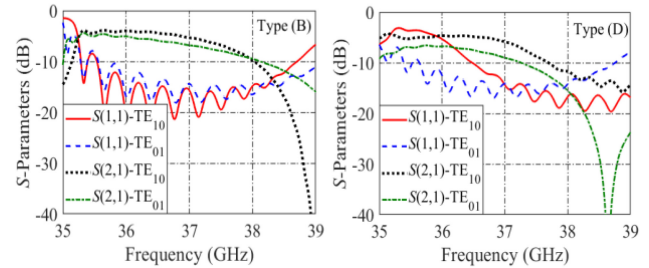


FIGURE 5. Simulated radiation pattern (gain in dB) of two SIW-DP-LWAs based on type B and D SIW-LWA's unit-cells of Fig. 3 at f = 38GHz.



FIGURE 6. Simulated *S*-parameters of two SIW-DP-LWAs based on type B and D SIW-LWA's unit-cells of Fig. 3.

where m is the number of fast wave space harmonics in the frequency range of interest. One point that needs to be considered here is that the beam angle difference between similarly involved space harmonics of each propagating mode must comply with propagation constant difference value. The difference between their arcsine function can be written as:

$$\sin^{-1}\left(\frac{(\beta_{TE10} - \beta_{TE10})/m}{k_0}\right) \qquad (11)$$

To investigate the beam angle difference between the two modes of $TE_{10}$ and $TE_{01}$ and their related HSH, in Fig. 4 we plot the propagation constant difference of $TE_{10}$ and $TE_{01}$ modes of the two SIW-LWAs' unit-cells of Fig. 3 (types B and D). This analysis shows that the value of $\beta TE_{10}$ - $\beta TE_{01}$ in type B of the SIW-LWAs' unit-cell has a lower value compared to type D, which shows a good agreement with the geometrical unit-cell analysis of Figs. 2-3. To examine the validity of our analysis we choose a random frequency, i.e., 38GHz, to check the beam behavior of the two propagating modes in comparison. Based on Fig. 3, at f = 38GHz we have two space harmonics as fast waves, so m in (11) must be set to 2, and the value of $k_0$ is set to be 2.35. The value of $\beta TE_{01}$ - $\beta TE_{01}$ in Fig. 4 at f = 38GHz for unit-cell types B and D are 0.15 and 0.6, respectively. Dividing these values by 2 and putting them in the arcsine function of (11) give us the angle of 1.82° and 7.73° for SIW-LWAs' unit-cells type B and D, respectively. So, for type B of SIW-LWA's unit-cell in Fig. 3, we should expect that the beam angle difference between two n = −1 space harmonics related to the $TE_{10}$ and $TE_{01}$ modes must be 1.82° at f = 38GHz. Similar angle difference must be expected for two beams of n = −2 space harmonics at f = 38GHz in a type B unit-cell. On the other hand, for type D unit-cell, the expected angle difference is 7.73° at f = 38GHz for each pair of n ϵ [−1, −2] space harmonics. Fig. 5 shows the simulated radiation pattern of two SIW-LWAs based on type B and D of SIW-LWA's unit-cells in Fig. 3 (the length of the antennas considered to be more than $10\lambda_0$ in this example). Fig. 5 shows a 2° and 7° difference between each pair of beams for our LWAs based on type B and D unit-cells, respectively. This shows a good agreement with our unit-cell analysis of Figs. 3-4.

The analysis of Figs. 3-5 also show that we can feasibly shift the beams of each mode by choosing a suitable unit-cell (Type D) for our LWA with a careful analysis of the propagation constant behavior of the LWA's unit-cell. It should be mentioned that besides the study of the DP-LWA's unit-cell behavior, we also need to analyze its effect on the bandwidth for our antenna to make sure that the two propagating modes of our DP-LWA have roughly the same bandwidth operation. Fig. 6 shows the simulated S-parameter responses of two LWAs based on type B and D unit-cells of the previous example (the antenna length is considered to be $10\lambda_0$ in this analysis). The analysis of Fig. 6 shows that the type B DP-LWA can provide a better alignment between the S-parameter responses compared to the type D for the two propagating modes of $TE_{10}$ and $TE_{01}$. Thus, it is chosen in the fabricated prototype.

### D. EXPERIMENTAL VALIDATION AND CONFIGURATION OF SIW-DP-LWA

The geometry of the designed SIW-DP-LWA is shown in Fig. 7. Here we utilized PSC-OMT as a compact feeding network since it provides two orthogonal modes of $TE_{10}$ and $TE_{01}$. The dimensions of the PSC-OMT were calculated based on the analysis of [61] and applied to the proposed design. In addition, a transition between the PSC-OMT and the WR28 waveguide is designed to support the operation over the frequency range of interest ($35 < f_{GHz} < 39$). Here we use a triangular shape for our transition section (taper section) with the length of 9mm where we removed the top and bottom copper layer of the substrate. This transition is used on both ports of the PSC-OMT along its vertical and horizontal axes for the excitation of $TE_{10}$ and $TE_{01}$ modes, respectively. For the LWA section, we used a type B cross
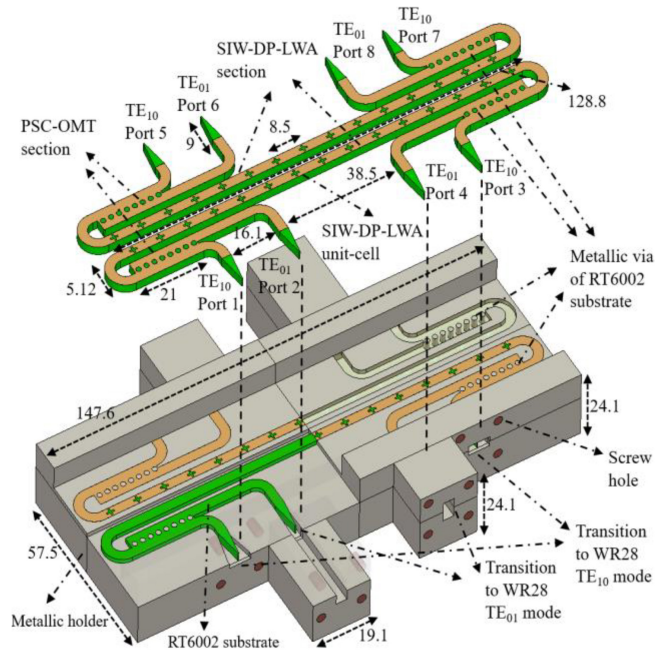
**FIGURE 7.** Schematic design of SIW-DP-LWA with the PCS-OMT and transition section to WR28 (all dimensions are in mm).



**FIGURE 8.** (a) Top view of fabricated SIW-DP-LWA prototype with PCS-OMT and transition section to WR28, (b) side view, and (c) measurement setup in a quasi-far-field chamber.

slot radiating element. The length of the LWA's section is considered to be more than $10\lambda_0$ in this analysis. In addition, due to the reciprocal behavior of HSH in the Brillouin diagram analysis of Fig. 3, we used two sets of SIW-DP-LWAs in this design to have a symmetric multi-beam radiation for our antenna. Fig. 8 shows the fabricated prototype of the SIW-DP-LWA with the PCS-OMT and transition section to WR28. The dielectric material used in this design is RT6002 with a dielectric constant of $\varepsilon_r = 2.94$ and thickness of 3mm. In addition, we also applied a metal epoxy in the via section of the PSC-OMT in order to ensure the via's wall is well covered with metal to keep the antenna performance acceptable. The type B cross slot has transverse and longitudinal slots lengths of 2.2mm and 2.5mm, respectively, with a width of 0.5mm. Figs. 9 (a)-(b) show simulated and measured $S$-parameters of the proposed SIW-DP-LWA for ports 1-2 and ports 7-8, respectively. The measured reflection coefficients of $TE_{10}$ (port 1 and 7) and $TE_{01}$ (port 2 and 8) modes for the antenna are below $-10$dB for the frequency ranges of $35.3 < f_{GHz} < 38.9$ and $35.7 < f_{GHz} < 38.7$, respectively. This shows that the two propagating modes have an approximately similar bandwidth behavior for our DP-LWA. In addition, the simulated and measured leakage ratio of the antenna for the two propagating modes has approximately similar behavior. There is a small discrepancy between the measured and simulated results due to fabrication tolerances. According to the analysis of Fig. 3(a), it is expected to have one proper beam ($n = -2$) and one improper beam ($n = -1$) for our antenna. Fig. 10 shows the antenna radiation patterns at two frequencies; $f = 36.5$GHz and $f = 38.4$GHz for the two propagating modes of $TE_{10}$ and $TE_{01}$ where we have one backward beam and one forward
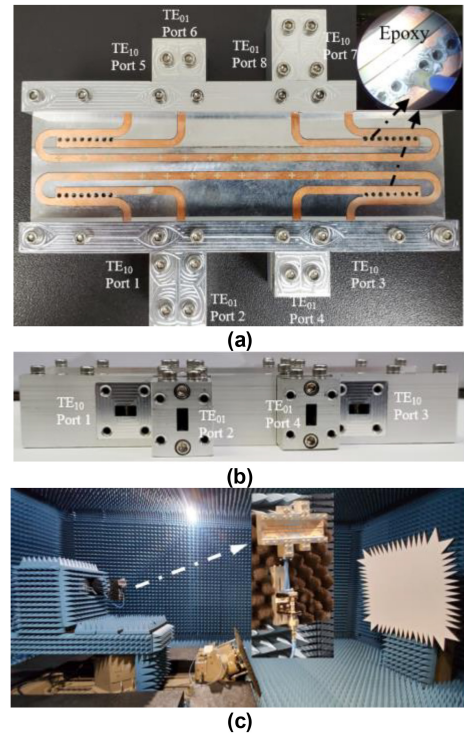
beam through the whole frequency range of the antenna. The peak gains of HSH ($n \in [-1, -32]$) for both modes of $TE_{10}$ and $TE_{01}$ are 15.3dB and 15.1dB, respectively. Besides, based on the analysis of Fig. 3(a), we expect that for both modes the beam related to the $n = -2$ space harmonics scans faster than the $n = -1$ space harmonic beam since the arcsine function variation of $\beta_{-2}/k_0$ is closer to 1 compared to the $\beta_{-1}/k_0$. This behavior is also validated in Fig. 10, in which the beam of $n = -2$ space harmonic covers more angles than the beam of $n = -1$ space harmonic for the same frequency variation. Here the measured scanning ranges of $n \in [-1, -2]$ space harmonics are $4°$ to $22°$ and $-67°$ to $-33$, respectively, which shows a good agreement with the ratio analysis of arcsine $\beta_{-n}/k_0$ of Fig. 3(a). In addition, based on the analysis of Fig. 4, a misalignment is expected between the beams of $TE_{10}$ and $TE_{01}$ modes for our antenna. Fig. 10 also shows that we have a $2°$ mismatch alignment between the beams of $TE_{10}$ and $TE_{01}$ modes. Thus, a good agreement is observed between the analysis, simulations, and measurement results of the proposed DP-SIW-LWA in which a wide scanning range can be achieved by using the HSH ($n \in [-1, -2]$) concept.

## III. DP LWA WITH FIXED AND SCANNING BEAM CAPABILITY
### A. ANALYSIS AND MODELING
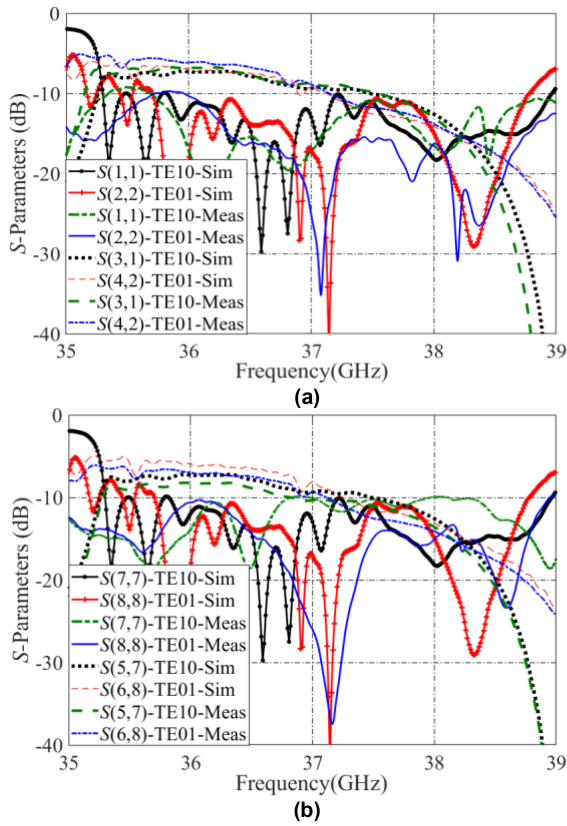A DPA based on its radiation mechanism can be divided into two categories: a DPA with fix beam operation and

**FIGURE 9.** Simulated and measured S-parameter response of $TE_{10}$ and $TE_{01}$ modes of (a) ports 1 and 2, and (b) ports 7-8.
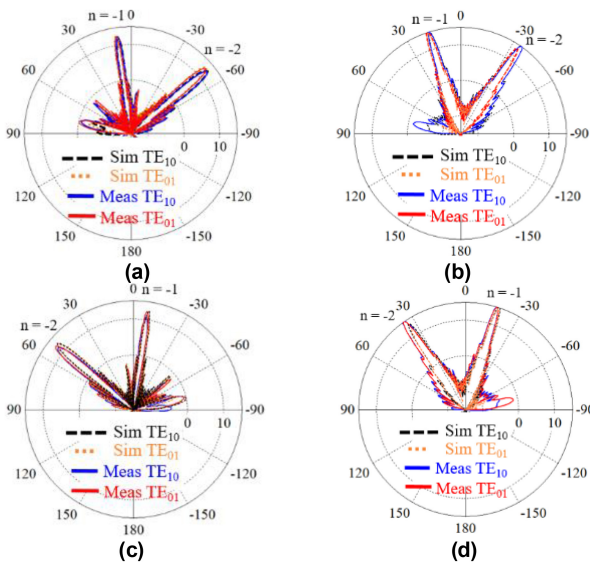


**FIGURE 10.** Simulated and measured E-plane co-polar radiation patterns (gain in dB) of SIW-DP-LWA of $TE_{10}$ and $TE_{01}$ modes of (a) ports 1 and 2 at f = 36.5GHz 2, (b) ports 1-2 at f = 38.4GHz, (c) ports 7 and 8 at f = 36.5GHz, and (d) ports 7-8 at f = 38.4GHz.

a DPA with scanning beam operation. To the best of the authors' knowledge, a DPA with the capability of both scanning and fixed beam operations does not exist in literature. Therefore, in this work, we demonstrate an DPA with fixed

and scanning beam capabilities by using the HSH concept. The core idea of the proposed design is to assign a specific task (scan or fix) to each polarization of the proposed DP-LWA. However, several aspects need to be analyzed and their trade off needs to be investigated. In the proposed design, first, we need to choose the topology of each polarization and decide about their function and operation task. In addition, other antenna characteristics such as gain level alignment and gain stability between each polarization need to be analyzed. In the proposed design and as a first step, we chose to assign the scanning and fixed beam operations to the $TE_{01}$ and $TE_{10}$ modes, respectively.

In the second step, we analyze the Brillouin diagram with the unit-cell geometrical effect (periodicity) on the antenna performances. From that, we can predict the HSH behavior in the fast wave region and evaluate the scanning range variation. The total behavior of the scanning range in periodic LWAs is predictable based on the arcsine function analysis. This function has two specific features when applied in the analysis of periodic LWAs. First, as long as we keep the ratio of $\beta_n/k_0$ close to zero in the frequency range of the antenna, we expect the scanning range variation related to the involved space harmonic not to vary too much due to the specific behavior of the arcsine function. However, periodic LWAs usually encounter the stopband issue when the ratio of $\beta_n/k_0$ approaches zero. Therefore, using this feature of the arcsine function to overcome the wide scanning range requires applying methods to suppress the open stopband problem, such as a phase reversal technique [62], impedance matched unit cells [56], [63], [64], and reflection cancelation [65]. The second feature of the arcsine function, which can be applied to overcome the limitation of a wide scanning range in periodic LWAs is the possibility of decreasing the variation of $\beta_n/k_0$ in the passband frequency range operation of the antenna, leading to the decrease in the scanning range variation. Since the scope of this work is not focused on the band edge issue of periodic LWAs, we chose to investigate the possibility of applying the second feature to our antenna.

From the analysis of Fig. 3(a), the scanning range variation of n = −1 space harmonic decrease at the third passband frequencies (f ≥ 35GHz) compared to lower ones. This is due to the higher value of $k_0$ which decrease the variation of $\beta_{-1}/k_0$. On the other hand, the n = −2 space harmonic has a wide scanning range variation compared to the n = −1 space harmonic in the third passband as the variation of $\beta_{-2}/k_0$ is close to 1. Thus, there is a possibility of decreasing the scanning range variation of the n = −2 space harmonic by approaching the fourth or higher passband since the ratio of $\beta_{-2}/k_0$ will be decreased. Fig. 11 shows the Brillouin diagram analysis of a one-dimensional periodic SIW-LWA with 5 passbands (periodicity, dielectric propagating medium, and effective width are 17mm, 2.94, and 3mm, respectively). Here we are interested in setting our analysis for the upper frequency range of Ka-band (f ≥ 36GHz). Therefore, based on the analysis of Fig. 11, the fundamental space harmonic
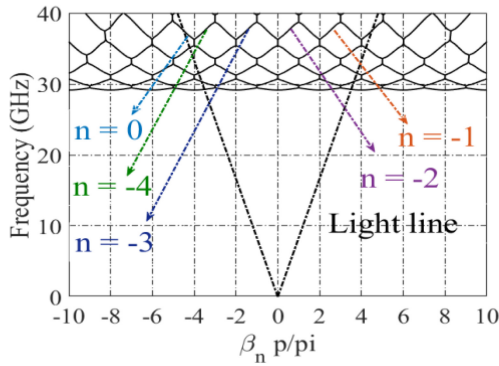
**FIGURE 11.** Brillouin diagram for a 1D-periodic SIW-LWA with periodicity of p = 17mm on a dielectric propagating medium of $\varepsilon_r$ = 2.94 and effective width of 3mm.

(n = 0) remains a slow wave, and we have 4 HSHs as fast waves (n $\epsilon$ [−1, −2, −3, −4]). The ratio of $\beta_n/k_0$ for n $\epsilon$ [−1, −2, −3, −4] space harmonics for 36 < $f_{GHz}$ < 38 in the fifth passband are [−0.54, −0.64], [−0.08, −0.15], [0.41, 0.33], [0.89, 0.84], respectively, which correspond to the angles [−33°, −39°], [−4°, −8°], [24°, 19°], [63°, 57°], respectively. Besides, the analysis of Fig. 11 also shows that the n = −2 space harmonic has the lowest scanning range variation in the fifth passband since its propagation constant is located near the center of the Brillouin diagram, resulting in the lowest value and variation ratio of $\beta_n/k_0$. Thus, we expect to have very low scanning range variation (around 5°) for our antenna in the frequency range of interest (36 < $f_{GHz}$ < 38).

A point that needs to be considered here is that the topology of applying scanning and fixed beam operation requires different periodicities (based on Brillouin diagram analysis of Fig. 3 and Fig. 11). Thus, to avoid modifying the geometrical shape of the antenna radiating element, we should choose the periodicity ratio between both polarizations as $PTE_{01}/PTE_{10}$ = 0.5 or $PTE_{10}/PTE_{01}$ = 2. Besides, taking the periodicity into the consideration for the proposed DP-LWA has a direct effect on the number of radiating elements for each polarization. Since one polarization has a higher number of radiating elements. Therefore, as a first estimation, we should expect to have a higher gain for one polarization compared to the other (if only we judge based on the radiating element number). A point that needs to be considered is that we also need to evaluate the effect and influence of the radiating elements on the antenna performances for both operating modes of $TE_{01}$ and $TE_{10}$ especially when we are dealing with the dually polarized operation.

To investigate this effect and as a third step, we analyze the geometrical effect of the radiating elements on the radiated power response of each polarization ($TE_{10}$ and $TE_{01}$ modes). First, we consider a symmetric cross slot and its longitudinal slot as our radiating element where they are assigned to the $TE_{10}$ and $TE_{01}$ modes, respectively ($TE_{01}$ and $TE_{10}$ modes are assigned to the Brillouin diagram of Fig. 3 and Fig. 11, respectively). Fig. 12 shows the radiated power response of these unit-cells for the frequency range of



(a)



(b)
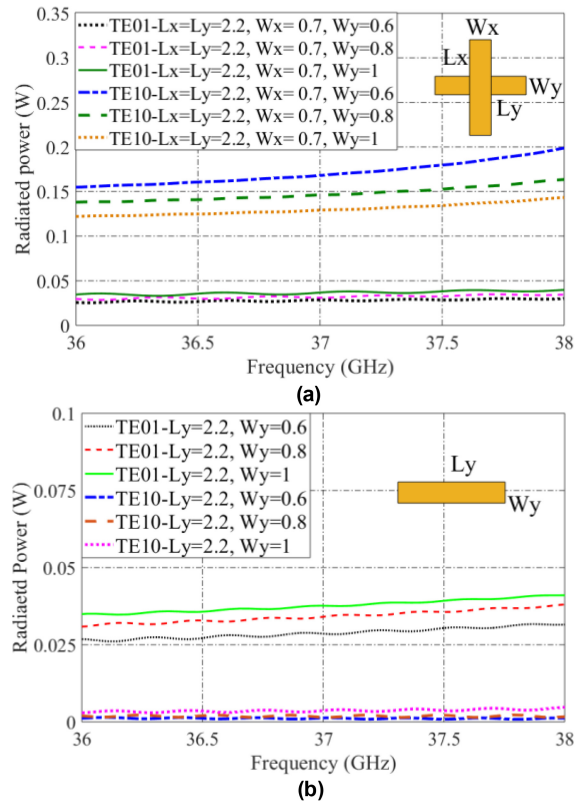
**FIGURE 12.** Effect of longitudinal slot width variation to the radiated power responses of $TE_{10}$ and $TE_{01}$ modes for the case of (a) a cross slot, and (b) a longitudinal slot. Input power is 0.5W.

interest (36 < $f_{GHz}$ < 38). This analysis shows that the $TE_{01}$ and $TE_{10}$ radiated power responses have different behavior for each of these unit-cells. The $TE_{10}$ mode has a higher radiated power compared to the $TE_{01}$ mode for the case of a symmetric cross slot, while for the case of a longitudinal slot it has much less radiated power compared to the $TE_{01}$ mode. A point that needs to be considered here is that the $TE_{01}$ mode has an approximate similar response for both radiating elements (symmetric cross slot and longitudinal slot) and its slope variation is not sharp, while the slope variation for the $TE_{10}$ has a sharp variation for the case of a symmetric cross slot which results in more gain variation for this antenna polarization ($TE_{10}$ mode). To overcome this issue, we investigated the geometrical effect of our radiating elements on their radiated power response for two polarizations of our DP-LWA. In this regard, we analyzed the effect of slot width variation on the radiated power responses of $TE_{10}$ and $TE_{01}$ modes for the case of a cross-slot and a longitudinal slot. The analysis of Fig. 12 shows that the radiated power response of $TE_{01}$ mode is increased by increasing the longitudinal slot width for both cases of cross slot and longitudinal slot. However, for the case of $TE_{10}$ mode, the radiated power response will decrease for the case of the asymmetric cross slot while it remains close to zero for the case of a longitudinal slot and it is much less compared to the $TE_{01}$ mode. It should be mentioned that in addition to the LWA unit-cell analysis, we also need
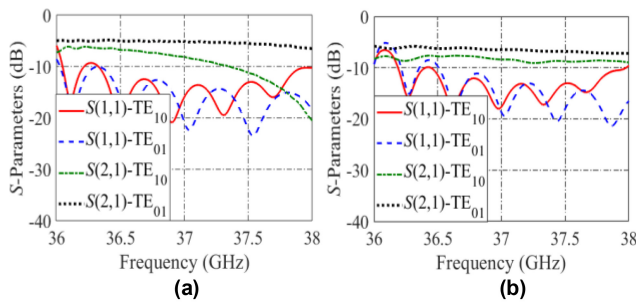
**FIGURE 13.** (a) S-parameters responses of a DP-LWA with symmetric cross slot ($Lx = 2.2$, $Ly = 2.2$, $Wx = 0.7$, $Wy = 0.7$) with a longitudinal slot ($Ly = 2.2$, $Wy = 0.7$), and (b) S-parameters responses of a DP-LWA with an asymmetric cross slot ($Lx = 2.2$, $Ly = 2.2$, $Wx = 0.7$, $Wy = 1$) with a longitudinal slot ($Ly = 2.2$, $Wy = 1$). All dimensions are in mm.
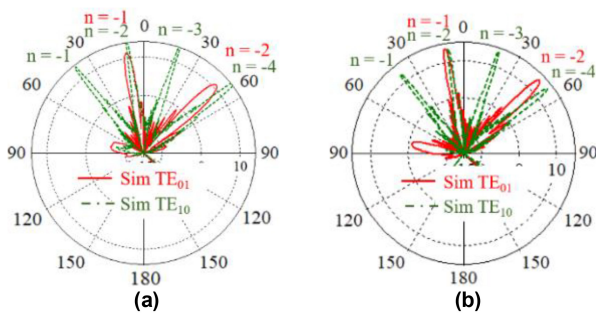


**FIGURE 14.** Simulated radiation pattern of DP-LWA at $f = 37.5$GHz based on (a) Fig. 13(a) analysis, and (b) based on Fig. 13(b) analysis.

to check the *S*-parameter response of each antenna polarization to ensure that the DPA has an acceptable performance. Fig. 13 (a)-(b) show the *S*-parameters responses for the case of DP-LWA with symmetric and asymmetric unit-cells, respectively (dimensions of LWA unit-cells specified in the capture of Fig. 13). The analysis of Fig. 13 shows that the antenna polarization related to the $TE_{10}$ mode has a narrower bandwidth compared to the $TE_{01}$ mode since it has a narrower passband frequency range. This shows a good agreement with the Brillouin diagram analysis of Fig. 11 and Fig. 3. In addition, *S*-parameters responses ($S21$) related to the $TE_{10}$ mode for the case of LWA with symmetric unit-cell have a sharper variation compared to the $TE_{01}$ mode, while both modes have smooth variation for the case of LWA with asymmetric unit-cell. In this regard, we should expect to have a mismatch between the gain level of each antenna polarization for the case of LWA with symmetric unit-cell. Besides, From Fig. 13 (b) it is expected that the beam levels of $TE_{10}$ and $TE_{01}$ modes have approximately similar levels since the radiated power of $TE_{10}$ mode (with four beams) is around 3 dB higher than $TE_{01}$ mode (with two beams). Fig. 14 shows the simulated radiation pattern response (gain in dB) of the DP-LWA at $f = 37.5$GHz based on the analysis of Fig 13. The analysis of Fig. 14 shows that for both LWAs cases (with symmetric and asymmetric unit-cell), we have one proper beam ($n = -2$) and one improper beam ($n = -1$) for the $TE_{01}$ mode while we have two proper beams ($n \in [-1, -2]$) and two improper beams ($n \in [-3, -4]$)
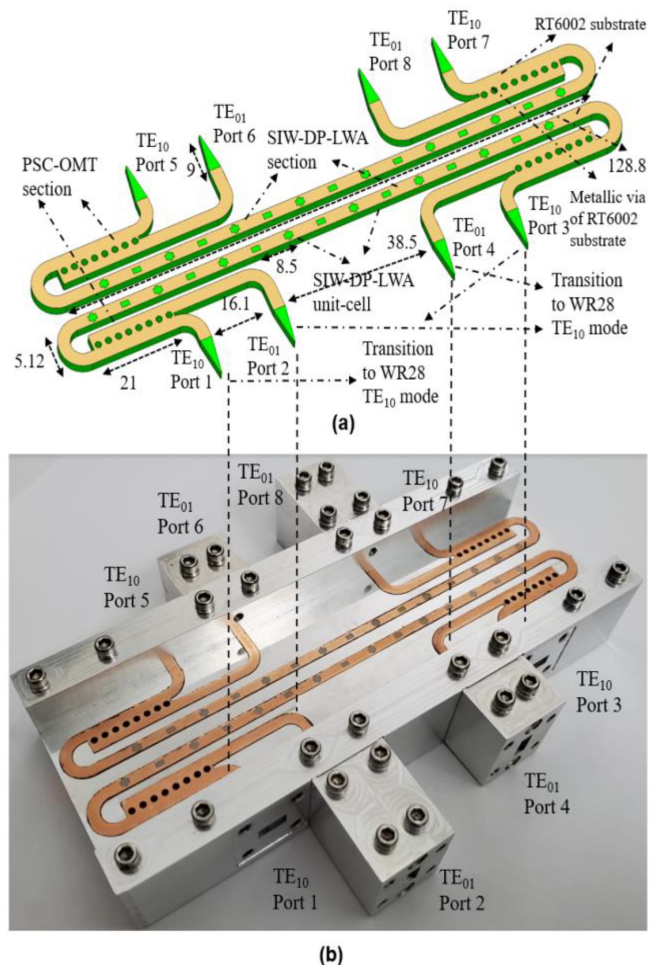


**FIGURE 15.** (a) Model of SIW-DP-LWA with fixed and scanning beam capabilities with and transition section to WR28, and (b) fabricated prototype.

for the $TE_{10}$ mode. This shows a good agreement with the Brillouin diagram analysis of Figs. 11 and 3. Besides, these analyses show that we have a mismatch between the gain level of each polarization for the case of LWA with symmetric unit-cell (4.2dB difference). However, a good gain alignment is observed between the antenna polarization for the case of LWA with asymmetric unit-cell (0.1dB difference). This shows a good agreement with the analysis of Figs. 12-13. Thus, with a careful analysis of Brillouin diagrams and their related unit-cells, we are able to achieve a DPA with fixed and scanning beam capabilities. We could also assign the features of scanning and fixed beam operations to the $TE_{10}$ and $TE_{01}$ modes, respectively. However, the use different radiation elements will be required for our DPA to find a suitable tradeoff between the antenna characteristics of the two propagating modes. In Section III-B we validate our analysis by showing a prototype of the proposed DP-SIW-LWA. Such a dual operation can be beneficial in next-generation access points.
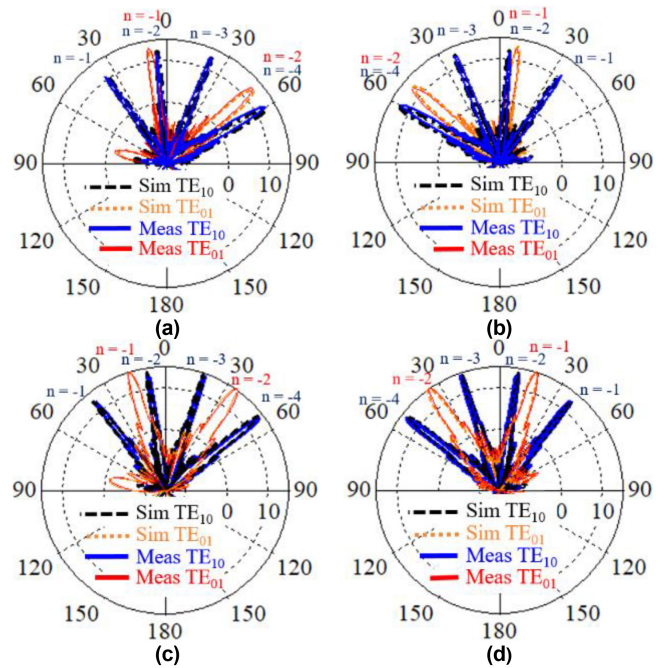
### B. VALIDATION AND PROTOTYPE
Fig. 15 shows the design prototype of the proposed SIW-DP-LWA with simultaneous fixed and scanning beam

**(a)**



**(b)**
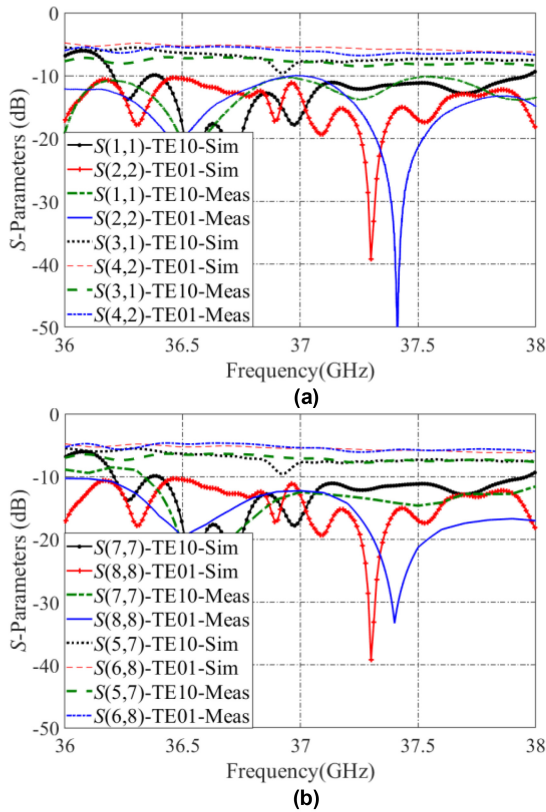
**FIGURE 16.** Simulated and measured S-parameter response of $TE_{10}$ and $TE_{01}$ modes of (a) ports 1 and 2, and (b) ports 7-8.



**(a)**



**(b)**



**(c)**



**(d)**

**FIGURE 17.** Simulated and measured E-plane co-polar radiation patterns (gain in dB) of SIW-DP-LWA of $TE_{10}$ and $TE_{01}$ modes of (a) ports 1 and 2 at f = 36.5GHz 2, (b) ports 7 and 8 at f = 36.5GHz, (c) ports 1 and 2 at f = 37.5GHz, and (d) ports 7 and 8 at f = 37.5GHz.

capabilities. Here, we again use a PSC-OMT for our DPA. The dielectric material used in this design is RT6002 with a dielectric constant of $\varepsilon_r = 2.94$ and thickness of 3mm. In the proposed DPA's prototype and the SIW-LWA's section, we use two sets of radiating elements in which we assign the periodicity of 17mm and 8.5mm to each. The first radiating element is an asymmetric cross slot in which the length of the transverse and longitudinal slot dimensions are set to 2.2mm, and their widths are set to 0.7mm and 1mm, respectively. The second radiating element is a longitudinal slot with length and width of 2.2mm and 1mm, respectively.

Figs. 16 (a)-(b) show the simulated and measured S-parameters response of the proposed SIW-DP-LWA for ports 1-2 and ports 7-8, respectively. The measured reflection coefficients of the $TE_{10}$ (port 1 and 7) and $TE_{01}$ (port 2 and 8) modes for the antenna are below $-10$dB for the frequency ranges of $36.35 < f_{GHz} < 38$ and $36 < f_{GHz} < 38$, respectively. There is a small discrepancy between the measured and simulated results due to fabrication tolerances. According to Fig. 3(a) and Fig. 11, it is expected to have two improper beams ($n \in [-1, -2]$) and two proper beams ($n \in [-1, -2]$) for the $TE_{10}$ mode and one proper beam ($n = -2$) with one improper beam ($n = -1$) for the $TE_{01}$ mode of our DP-LWA. In addition, we used two sets of DP-LWA in this design to have a symmetric multi-beam radiation for our antenna. Fig. 17 shows the antenna
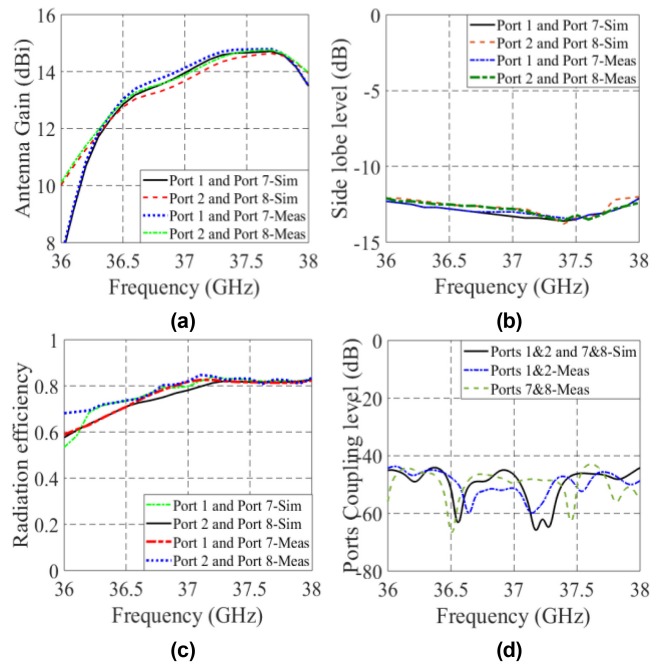
radiation patterns at the two frequencies of f = 36.5GHz and f = 37.5GHz for two propagating modes of $TE_{10}$ and $TE_{01}$. Here we have two forward beams and two backward beams for the $TE_{10}$ mode and one backward beam with one forward beam for the $TE_{01}$ mode of our antenna. Besides, based on Fig. 3(a), we should expect that the beam related to the $n = -2$ space harmonic of the $TE_{01}$ mode scans faster than the $n = -1$ space harmonic beam of this mode since the arcsine function variation of $\beta_{-2}/k_0$ is closer to 1 compared to the $\beta_{-1}/k_0$. In addition, Fig. 11 predicts to have a very low scanning range variation for each of HSH's beams of the $TE_{10}$ mode since the variation of $\beta_n/k_0$ of this mode is very low, and they are not close to 1. Fig. 17 also validates this behavior. Here the measured scanning ranges of $n \in [-1, -2]$ space harmonics of the $TE_{01}$ mode are $4°$ to $22°$ and $-67°$ to $-33°$, respectively. For the $TE_{10}$ mode we have [$5°$, $4°$, $5°$, $6°$] angle beam's variation for $n \in [-1, -2, -3, -4]$, respectively. This shows a good agreement with the ratio analysis of the arcsine $\beta_n/k_0$ in Fig. 3(a) and Fig. 11. In addition, the scanning range variation for the fixed beam operation in this work is in an acceptable range compared to the scanning range variation in [57] and [66], which have around $12°$ variation. Thus, an agreement observed between the analysis, simulation, and measurement results of the proposed DP-LWA in which the simultaneous fixed and scanning features are achieved by using the PSC mechanism and the HSH concept. Fig. 18(a) also shows the antenna gain performance for each polarization of the proposed DP-LWA. The peak gains for both $TE_{10}$ and $TE_{01}$ modes are 14.8dBi and 14.6dBi, respectively. An acceptable gain alignment is observed

**TABLE 1.** Comparison of proposed SIW-DP-LWA with other LWAS.

| Ref. | Antenna Type | Antenna Polarization | Antenna Feature | Max Scanning Variation for each polarization (degree) | Antenna Bandwidth (GHz) | Max Eff (%) |
|---|---|---|---|---|---|---|
| [39] | Plasmon Polariton LWA | Dual-Polarized Single beam | Scanning | 49 / 63 | 6 | - |
| [40] | SIW LWA | Dual-Polarized Single beam | scanning | 60 / 73 | 2.8 | - |
| [52] | Glide Symmetric Prism LWA | Single-Polarized Single-Beam | Fixed | 2 | 8 | 90 |
| [57] | Reflector-LWA | Single-polarized | Fixed | 12 | 2 | 80 |
| [66] | Reflector-LWA | Dual Polarized Single-Beam | Fixed | 11 / 11 | 2 | 94 |
| [58] | Dispersive Symmetric Prism-LWA | Single-Polarized Multi-Beam | Fixed | 2 | 10 | 90 |
| **This Work** | **SIW-LWA** | **Dual-Polarized Multi-Beam** | **Scanning** | **34 / 34** | **4** | **84** |
| **This Work** | **SIW-LWA** | **Dual-Polarized Multi-Beam** | **Fixed and Scanning** | **5 / 34** | **2** | **84** |



**FIGURE 18.** Simulated and measured (a) antenna gain (in dBi), (b) side lobe level, (c) radiation efficiency, and (d) ports coupling level of the proposed SIW-DP-LWA prototype of Figure. 15.

between those polarizations. This shows a good agreement with the unit-cell radiated power analyses of Fig. 12. The maximum gain difference between the beams related to the $TE_{10}$ and $TE_{01}$ modes are 0.2dB and 0.3dB, respectively (the gain values presented in Fig. 18(a) are the average values of the beams of $TE_{10}$ and $TE_{01}$ modes). Fig. 18(b) provides the side lobe level (SLL) of each polarization where they are operating in an acceptable range better than −12dB over the whole operating frequency range. Fig. 18(c) gives the radiation efficiency where a good agreement is observed for both polarizations. A maximum radiation efficiency of 84% is obtained for each polarization. Besides, a high level of coupling between antenna ports could be highly beneficial to reduce the effects of interference. Fig. 18(d) shows the port coupling level of the proposed antenna. A coupling level better than -40dB is observed for the whole operating frequency range. Table 1 shows the comparison between proposed work and others LWAs. The work presented in Section II (LWA with scanning feature) achieves more bandwidth and lower scanning range compared to [40] while these features improved in [39] by using a plasmon polariton LWA. The works of [39], [40] generated a single beam while

the work presented here can provide multi-beam operation from each antenna polarization which can improve the link reliability and availability [53]. Besides, the antenna demonstrated in Section III takes the benefit of shrinking the size and achieving a lower scanning range variation compared to the reflector based LWAs in [57], [66] for the case of a fixed beam operation. On the other hand, using dispersive symmetric prism [58] and glide symmetric prism [52] can provide a lower scanning range and wider bandwidth at the expense of a larger geometry for the antenna to achieve a fixed beam operation. Finally, this work demonstrates a combination of fixed and scanning beam operations which can reduce the volume and size of wireless communication systems, thereby presenting an alternative solution for future broadcasting and wireless developments.

## IV. CONCLUSION

The concept of applying HSHs in a hybrid form of the NRD waveguide and the square SIW structure for the $TE_{10}$ and $TE_{01}$ modes is proposed and applied to several theoretical and experimental prototypes in this work. The properties of polarization diversity related to the unit-cell geometrical structures for different features of an LWA are investigated. It is shown that the propagation constant of the $TE_{10}$ and $TE_{01}$ modes can be manipulated by the geometrical structure of the LWA's radiating element for achieving the design flexibility of the proposed antenna. In addition, the effect of the difference between the two propagation constants for the two modes $TE_{10}$ and $TE_{01}$ on the beam alignment of their related HSHs is investigated. Besides, the feasibility of even and odd HSHs (n ϵ [−1, −2, −3, −4]) of the two

propagating modes ($TE_{10}$ and $TE_{01}$) in different passbands is studied, where we show that the features of scanning and fixed beam operations are achievable with a careful analysis of the Brillouin diagram and propagation constant variation of each HSH. In this regard, the PSC mechanism along with the HSH concept is used in this work to demonstrate a multifunctional SIW-DP-LWA with the capability of simultaneous fixed and scanning multi-beam operations. In this work, two experimental prototypes of the proposed antennas are shown as proofs of concept to validate the analysis method formulated in this work. The measured results show a good agreement with simulated counterparts, thus validating the proposed LWAs.

## REFERENCES

[1] B. D. Braaten, S. Roy, I. Irfanullah, S. Nariyal, and D. E. Anagnostou, "Phase-compensated conformal antennas for changing spherical surfaces," *IEEE Trans. Antennas Propag.*, vol. 62, no. 4, pp. 1880–1887, Apr. 2014.

[2] G. Han, B. Du, W. Wu, and B. Yang, "A novel hybrid phased array antenna for satellite communication on-the-move in Ku-band," *IEEE Trans. Antennas Propag.*, vol. 63, no. 4, pp. 1375–1383, Apr. 2015.

[3] T. Hong, Z. Zhao, W. Jiang, S. Xia, Y. Liu, and S. Gong, "Dualband SIW cavity-backed slot array using TM020 and TM120 modes for 5G applications," *IEEE Trans. Antennas Propag.*, vol. 67, no. 5, pp. 3490–3495, May 2019.

[4] L. A. A. Oliner and D. R. Jackson, "Leaky-wave antennas," in *Antenna Engineering Handbook*, 5th ed., J. L. Volakis, Ed. New York, NY, USA: McGraw-Hill, 2018, ch. 15.

[5] N. Hines and J. R. Upson, "A wide aperture tapered-depth scanning antenna," Ohio state Univ. Res. Found., Columbus, OH, USA, Rep. 667-7, Dec. 1957.

[6] C. A. Balanis, "Leaky-wave antennas," in *Modern Antenna Handbook*. Somerset, NJ, USA: Wiley Telecom, p. 338.

[7] J. Liu, D. R. Jackson, and Y. Long, "Substrate integrated waveguide (SIW) leaky-wave antenna with transverse slots," *IEEE Trans. Antennas Propag.*, vol. 60, no. 1, pp. 20–29, Jan. 2012.

[8] Y. Mohtashami and J. Rashed-Mohassel, "A butterfly substrate integrated waveguide leaky-wave antenna," *IEEE Trans. Antennas Propag.*, vol. 62, no. 6, pp. 3384–3388, Jun. 2014.

[9] R. Honey, "A flush-mounted leaky-wave antenna with predictable patterns," *IRE Trans. Antennas Propag.*, vol. 7, no. 4, pp. 320–329, Oct. 1959.

[10] F. Xu and K. Wu, "Understanding leaky-wave structures: A special form of guided-wave structure," *IEEE Microw. Mag.*, vol. 14, no. 5, pp. 87–96, Jul./Aug. 2013.

[11] M. R. Rahimi, N. Bayat-Makou, and A. A. Kishk, "Millimeterwave substrate integrated gap waveguide leaky-wave antenna for WiGig applications," *IEEE Trans. Antennas Propag.*, vol. 67, no. 9, pp. 5790–5800, Sep. 2019.

[12] Y. Lyu *et al.*, "Leaky-wave antennas based on noncutoff substrate integrated waveguide supporting beam scanning from backward to forward," *IEEE Trans. Antennas Propag.*, vol. 64, no. 6, pp. 2155–2164, Jun. 2016.

[13] D. Shin, D. Jung, D. Kim, J. Ham, and S. Park, "A distributed FMCW radar system based on fiber-optic links for small drone detection," *IEEE Trans. Instrum. Meas.*, vol. 66, no. 2, pp. 340–347, Feb. 2017.

[14] A. Neto, M. Ettorre, G. Gerini, and P. De Maagt, "Leaky wave enhanced feeds for multibeam reflectors to be used for telecom satellite based links," *IEEE Trans. Antennas Propag.*, vol. 60, no. 1, pp. 110–120, Jan. 2012.

[15] K. Murata, I. Watanabe, A. Kasamatsu, T. Tanaka, and Y. Monnai, "Sparse 3D imaging using terahertz leaky-wave radar," in *Proc. 42nd Int. Conf. Infrared, Millimeter, Terahertz Waves (IRMMW-THz)*, 2017, pp. 1–2.

[16] S. Yang and H. Ling, "Application of a microstrip leaky wave antenna for range–azimuth tracking of humans," *IEEE Geosci. Remote Sens. Lett.*, vol. 10, no. 6, pp. 1384–1388, Nov. 2013.

[17] Y. Li and J. Wang, "Polarization property of leaky coaxial cable with overlapped triangle slots," *IEEE Antennas Wireless Propag. Lett.*, vol. 9, pp. 1049–1052, 2010.

[18] A. M. Bøifot, E. Lier, and T. Schaug-Pettersen, "Simple and broadband orthomode transducer (antenna feed)," *IEE Proc. H Microw. Antennas Propag.*, vol. 137, no. 6, pp. 396–400, Dec. 1990.

[19] A. Navarrini and R. L. Plambeck, "A turnstile junction waveguide orthomode transducer," *IEEE Trans. Microw. Theory Techn.*, vol. 54, no. 1, pp. 272–277, Jan. 2006.

[20] G. Pisano *et al.*, "A broadband WR10 turnstile junction orthomode transducer," *IEEE Microw. Wireless Compon. Lett.*, vol. 17, no. 4, pp. 286–288, Apr. 2007.

[21] M. A. Abdelaal, S. I. Shams, M. A. Moharram, M. Elsaadany, and A. A. Kishk, "Compact full band OMT based on dual-mode doubleridge waveguide," *IEEE Trans. Microw. Theory Techn.*, vol. 66, no. 6, pp. 2767–2774, Jun. 2018.

[22] M. A. Abdelaal and A. A. Kishk, "Ka-band 3-D-printed wideband groove gap waveguide orthomode transducer," *IEEE Trans. Microw. Theory Techn.*, vol. 67, no. 8, pp. 3361–3369, Aug. 2019.

[23] M. Esquius-Morote, M. Mattes, and J. R. Mosig, "Orthomode transducer and dual-polarized horn antenna in substrate integrated technology," *IEEE Trans. Antennas Propag.*, vol. 62, no. 10, pp. 4935–4944, Oct. 2014.

[24] H. Jin, Y. M. Huang, H. Jin, and K. Wu, "$S$-band substrate integrated waveguide orthomode transducer integrated with dualpolarized horn antenna," *IEEE Trans. Antennas Propag.*, vol. 66, no. 5, pp. 2291–2298, May 2018.

[25] Z. Zhang and K. Wu, "A wideband dual-polarized dielectric magnetoelectric dipole antenna," *IEEE Trans. Antennas Propag.*, vol. 66, no. 10, pp. 5590–5595, Oct. 2018.

[26] A. Dadgarpour, N. Bayat-Makou, M. A. Antoniades, A. A. Kishk, and A. Sebak, "A dual-polarized magnetoelectric dipole array based on printed ridge gap waveguide with dual-polarized split-ring resonator lens," *IEEE Trans. Antennas Propag.*, vol. 68, no. 5, pp. 3578–3585, May 2020.

[27] Y. Guo, K. Khoo, and L. C. Ong, "Wideband dual-polarized patch antenna with broadband baluns," *IEEE Trans. Antennas Propag.*, vol. 55, no. 1, pp. 78–83, Jan. 2007.

[28] K. L. Lau and K. M. Luk, "A wideband dual-polarized L-probe stacked patch antenna array," *IEEE Antennas Wireless Propag. Lett.*, vol. 6, pp. 529–532, 2007.

[29] H. Wong, K.-L. Lau, and K.-M. Luk, "Design of dual-polarized L-probe patch antenna arrays with high isolation," *IEEE Trans. Antennas Propag.*, vol. 52, no. 1, pp. 45–52, Jan. 2004.

[30] K.-L. Wong, H.-C. Tung, and T.-W. Chiou, "Broadband dual-polarized aperture-coupled patch antennas with modified H-shaped coupling slots," *IEEE Trans. Antennas Propag.*, vol. 50, no. 2, pp. 188–191, Feb. 2002.

[31] S.-C. Gao, L.-W. Li, M.-S. Leong, and T.-S. Yeo, "Dual-polarized slotcoupled planar antenna with wide bandwidth," *IEEE Trans. Antennas Propag.*, vol. 51, no. 3, pp. 441–448, Mar. 2003.

[32] C. Johnson, *5G New Radio in Bullet*, 1st ed. Farnham, U.K.: Independently Published, 2019. [Online]. Available: www.5g-bullets.com

[33] M. Enescu, *5G New Radio: A Beam-Based Air Interface*. Hoboken, NJ, USA: Wiley, 2020.

[34] J. Garrido-Holgado and J. L. Gómez-Tornero, "LTE low-cost vertical sectorization through a leaky-wave antenna," in *Proc. 8th Eur. Conf. Antennas Propag. (EuCAP)*, 2014, pp. 2061–2065.

[35] M. Garcia-Vigueras, M. Esquius-Morote, J. Perruisseau-Carrier, and J. R. Mosig, "Dual-beam radiation from ID leaky-wave antennas," in *Proc. 8th Eur. Conf. Antennas Propag. (EuCAP)*, 2014, pp. 1447–1450.

[36] Y. Zhu, Y. Chen, and S. Yang, "Decoupling and low-profile design of dual-band dual-polarized base station antennas using frequency-selective surface," *IEEE Trans. Antennas Propag.*, vol. 67, no. 8, pp. 5272–5281, Aug. 2019.

[37] Y.-W. Hsu, T.-C. Huang, H.-S. Lin, and Y.-C. Lin, "Dual-polarized quasi Yagi–Uda antennas with endfire radiation for millimeter-wave MIMO terminals," *IEEE Trans. Antennas Propag.*, vol. 65, no. 12, pp. 6282–6289, Dec. 2017.

[38] M. García-Vigueras, M. Esquius-Morote, and J. R. Mosig, "Dual-polarized directional antenna with application to polarimetric radar," in *Proc. IEEE Int. Symp. Antennas Propag. USNC/URSI Nat. Radio Sci. Meeting*, Vancouver, BC, Canada, 2015, pp. 27–28.

[39] H.-W. Yu, Y.-C. Jiao, C. Zhang, and Z.-B. Weng, "Dual-linearly polarized leaky-wave patch array with low cross-polarization levels using symmetrical spoof surface plasmon polariton lines," *IEEE Trans. Antennas Propag.*, vol. 69, no. 3, pp. 1781–1786, Mar. 2021, doi: 10.1109/TAP.2020.

[40] Q. Zhang, Q. Zhang, H. Liu, and C. H. Chan, "Dual-band and dual-polarized leaky-wave antenna based on slotted SIW," *IEEE Antennas Wireless Propag. Lett.*, vol. 18, no. 3, pp. 507–511, Mar. 2019.

[41] T. Debogović, J. Bartolić, and J. Perruisseau-Carrier, "Dual-polarized partially reflective surface antenna with MEMS-based beamwidth reconfiguration," *IEEE Trans. Antennas Propag.*, vol. 62, no. 1, pp. 228–236, Jan. 2014.

[42] G. Liu, X. Sun, X. Chen, D. Xiong, M. Li, and M.-C. Tang, "A broadband low-profile dual-linearly polarized dipole-driven metasurface antenna," *IEEE Antennas Wireless Propag. Lett.*, vol. 19, no. 10, pp. 1759–1763, Oct. 2020.

[43] O. Yurduseven, N. L. Juan, and A. Neto, "A dual-polarized leaky lens antenna for wideband focal plane arrays," *IEEE Trans. Antennas Propag.*, vol. 64, no. 8, pp. 3330–3337, Aug. 2016.

[44] W. Hong et al., "Multibeam antenna technologies for 5G wireless communications," *IEEE Trans. Antennas Propag.*, vol. 65, no. 12, pp. 6231–6249, Dec. 2017.

[45] M. A. Jasim, N. Siasi, A. Aldalbahi, and N. Ghani, "Soft self-handover scheme for mmWave communications," in *Proc. SoutheastCon*, 2019, pp. 1–6.

[46] A. Jaesim, A. Aldalbahi, N. Siasi, D. Oliveira, and N. Ghani, "Dual-beam analog beamforming for mmWave communications," in *Proc. IEEE 10th Annu. Ubiquitous Comput. Electron. Mobile Commun. Conf. (UEMCON)*, 2019, pp. 744–748.

[47] M. Jasim, J. E. Pezoa, and N. Ghani, "Simultaneous multi-beam analog beamforming and coded grating lobes for initial access in mmWave systems," in *Proc. CHILEAN Conf. Electr. Electron. Eng. Inf. Commun. Technol. (CHILECON)*, 2017, pp. 1–6.

[48] Y. Li and J. Wang, "Dual-band leaky-wave antenna based on dualmode composite microstrip line for microwave and millimeter-wave applications," *IEEE Trans. Antennas Propag.*, vol. 66, no. 4, pp. 1660–1668, Apr. 2018.

[49] W.-Y. Park and S. Lim, "Multi-beam leaky-wave antenna: Design, analysis, and experiments," *Electromagnetics*, vol. 31, no. 4, pp. 247–257, Jan. 2011.

[50] C.-C. Hu, C. F. Jsu, and J.-J. Wu, "An aperture-coupled linear microstrip leaky-wave antenna array with two-dimensional dual-beam scanning capability," *IEEE Trans. Antennas Propag.*, vol. 48, no. 6, pp. 909–913, Jun. 2000.

[51] T.-L. Chen and Y.-D. Lin, "Dual-beam microstrip leaky-wave array excited by aperture-coupling method," *IEEE Trans. Antennas Propag.*, vol. 51, no. 9, pp. 2496–2498, Sep. 2003.

[52] O. Zetterstrom, E. Pucci, P. Padilla, L. Wang, and O. Quevedo-Teruel, "Low-dispersive leaky-wave antennas for mmWave point-to-point high-throughput communications," *IEEE Trans. Antennas Propag.*, vol. 68, no. 3, pp. 1322–1331, Mar. 2020.

[53] A. Aldalbahi, N. Siasi, M. Ababneh, and M. Jasim, "Grating lobes for enhanced scattering intensity in millimeter wave sparse channels," in *Proc. IEEE 9th Annu. Comput. Commun. Workshop Conf. (CCWC)*, 2019, pp. 1010–1014.

[54] A. A. Sakr, W. M. Dyab, and K. Wu, "Theory of polarization-selective coupling and its application to design of planar orthomode transducers," *IEEE Trans. Antennas Propag.*, vol. 66, no. 2, pp. 749–762, Feb. 2018.

[55] A. A. Sakr, W. Dyab, and K. Wu, "Design methodologies of compact orthomode transducers based on mechanism of polarization selectivity," *IEEE Trans. Microw. Theory Techn.*, vol. 66, no. 3, pp. 1279–1290, Mar. 2018.

[56] M. R. Rahimi, M. S. Sharawi, and K. Wu, "Higher-order space harmonics in substrate integrated waveguide leaky-wave antennas," *IEEE Trans. Antennas Propag.*, vol. 69, no. 8, pp. 4332–4346, Aug. 2021, doi: 0.1109/TAP.2020.3048530.

[57] N. Bayat-Makou, K. Wu, and A. A. Kishk, "Single-layer substrate-integrated broadside leaky long-slot array antennas with embedded reflectors for 5G systems," *IEEE Trans. Antennas Propag.*, vol. 67, no. 12, pp. 7331–7339, Dec. 2019.

[58] Q. Chen, O. Zetterstrom, E. Pucci, A. Palomares-Caballero, P. Padilla, and O. Quevedo-Teruel, "Glide-symmetric holey leaky-wave antenna with low dispersion for 60 GHz point-to-point communications," *IEEE Trans. Antennas Propag.*, vol. 68, no. 3, pp. 1925–1936, Mar. 2020.

[59] J. L. G. Tornero and A. A. Melcon, "Nonorthogonality relations between complex hybrid modes: An application for the leaky-wave analysis of laterally shielded top-open planar transmission lines," *IEEE Trans. Microw. Theory Techn.*, vol. 52, no. 3, pp. 760–767, Mar. 2004.

[60] D. M. Pozar, *Microwave Engineering*. Hoboken, NJ, USA: Wiley, 2012.

[61] A. A. Sakr, W. M. Dyab, and K. Wu, "A dually polarized six-port junction based on polarization-selective coupling for polarization-inclusive remote sensing," *IEEE Trans. Microw. Theory Techn.*, vol. 66, no. 8, pp. 3817–3827, Aug. 2018.

[62] Z. L. Ma, L. J. Jiang, S. Gupta, and W. E. I. Sha, "Dispersion characteristics analysis of one dimensional multiple periodic structures and their applications to antennas," *IEEE Trans. Antennas Propag.*, vol. 63, no. 1, pp. 113–121, Jan. 2015.

[63] Y. Lyu, F. Meng, G. Yang, P. Wang, Q. Wu, and K. Wu, "Periodic leaky-wave antenna based on complementary pair of radiation elements," *IEEE Trans. Antennas Propag.*, vol. 66, no. 9, pp. 4503–4515, Sep. 2018.

[64] M. H. Rahmani and D. Deslandes, "Backward to forward scanning periodic leaky-wave antenna with wide scanning range," *IEEE Trans. Antennas Propag.*, vol. 65, no. 7, pp. 3326–3335, Jul. 2017.

[65] Y. Geng, J. Wang, Z. Li, Y. Li, M. Chen, and Z. Zhang, "Dual-beam and tri-band SIW leaky-wave antenna with wide beam scanning range including broadside direction," *IEEE Access*, vol. 7, pp. 176361–176368, 2019.

[66] Q.-C. Ye, Y.-M. Zhang, J.-L. Li, G. F. Pedersen, and S. Zhang, "High-isolation dual-polarized leaky-wave antenna with fixed beam for full-duplex millimeter-wave applications," *IEEE Trans. Antennas Propag.*, vol. 69, no. 11, pp. 7202–7212, Nov. 2021.
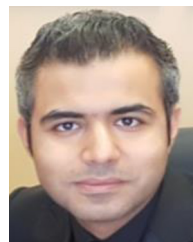
**MOHAMMAD REZA RAHIMI** (Student Member, IEEE) received the M.Sc. degree in electrical and computer engineering from Concordia University, Montreal, QC, Canada, in 2018. He is currently pursuing the Ph.D. degree with Polytechnique Montréal (University of Montreal), Montreal. He was a Research and a Teaching Assistant with Concordia University from 2015 to 2018, where he was with the Laboratory of Advanced Technology on Antenna and Microwave Systems from 2017 to 2018. In 2018, he joined the Poly-Grames Research Center with Polytechnique Montréal. His current research interests include massive MIMO subarray, beamforming network, dual-polarized multifunctional MIMO antennas, leaky-wave antennas, and integrated active antenna array. He has served as a Reviewer for the 2019 IEEE AP-S/URSI and the 2020 IEEE AP-S/URSI. His paper was awarded as a Finalist at the 2018 IEEE AP-S/URSI Conference.

**MOHAMMAD S. SHARAWI** (Senior Member, IEEE) is a Full Professor with the Electrical Engineering Department, University of Montreal (Polytechnique Montreal), Montreal, QC, Canada, where he is also a member of the Poly-Grames Research Center. He was with the King Fahd University of Petroleum and Minerals, Dhahran, Saudi Arabia, from 2009 to 2018, where he founded and directed the Antennas and Microwave Structure Design Laboratory. He was a Visiting Professor with the Intelligent Radio Laboratory, Department of Electrical Engineering, University of Calgary, Calgary, AB, Canada, in Summer 2014 to Fall 2014. He was a Visiting Research Professor with Oakland University, Rochester, MI, USA, in Summer 2013. He has more than 350 papers published in refereed journals and international conferences, 11 book chapters (two of which in the Antenna Handbook, 5th edition, McGraw Hill, 2018), one single authored book titled *Printed MIMO Antenna Engineering* (Artech House, 2014), and the lead author of the recent book '*Design and Applications of Active Integrated Antennas* (Artech House, 2018). He has 25 issued/granted and 12 pending patents in the U.S. Patent Office. His research interests include multiband printed multiple-input–multiple-output (MIMO) antenna systems, reconfigurable and active integrated antennas, millimeter-wave MIMO antennas and integrated 4G/5G antennas, microwave sensors, applied electromagnetics, and computational methods. He was a recipient of the Abdul Hameed Shoman Foundation Award for Arab researchers for the category of wireless systems in 2020 in addition to various best IEEE conference paper awards. He is also serving as an Associate Editor for the IEEE ANTENNAS AND WIRELESS PROPAGATION LETTERS, *IET Microwaves, Antennas and Propagation*, and IEEE OPEN JOURNAL ON ANTENNAS AND PROPAGATION and an Area Editor (Antennas and Microwave Devices and Systems) for *Microwave and Optical Technology Letters* (Wiley). He is also the Specialty Chief Editor for the newly launched *Frontiers in Communications and Networks* for the System and Test-Bed design section. He has served on the technical and organizational program committees and organized several special sessions on MIMO antenna systems and architectures in several international conferences, such as EuCAP, APS, IMWS-5G, APCAP, and iWAT among many others for many years. He is also the IEEE Antennas and Propagation Society Chair of the Montreal section and an active member of the IEEE Member benefits committee leading the initiative of the APS Student Travel Grant. He is also the regional delegate of the EuRAAP in North America.

**KE WU** (Fellow, IEEE) received the B.Sc. degree (Hons.) in radio engineering from the Nanjing Institute of Technology (currently Southeast University), Nanjing, China, in 1982, the D.E.A. degree (Hons.) and the Ph.D. degree (Hons.) in optics, optoelectronics, and microwave engineering from the Institut National Polytechnique de Grenoble and the University of Grenoble, Grenoble, France, in 1984 and 1987, respectively.

He was the Founding Director of the Center for Radio frequency Electronics Research of Quebec (Regroupement stratégique of FRQNT) and the Canada Research Chair of RF and Millimeter-Wave Engineering. He is currently a Professor of Electrical Engineering and the Industrial Research Chair of Future Wireless Technologies with Polytechnique Montréal (University of Montreal), where he is the Director of the Poly-Grames Research Center. He has authored or coauthored over 1400 referred articles and numerous books/book chapters, and filed over 80 patents. His current research interests involve substrate integrated circuits and systems, antenna arrays, field theory and joint field/circuit modeling, ultrafast interconnects, wireless power transmission and harvesting, microwave photonics, and MHz-through-THz technologies and transceivers, including RFICs/MMICs for multifunction wireless systems and biomedical applications.

Prof. Wu was a recipient of many awards and Prizes including the Inaugural IEEE MTT-S Outstanding Young Engineer Award, the 2004 Fessenden Medal of the IEEE Canada, the 2009 Thomas W. Eadie Medal of the Royal Society of Canada, the Queen Elizabeth II Diamond Jubilee Medal in 2013, the 2013 FCCP Education Foundation Award of Merit, the 2014 IEEE MTT-S Microwave Application Award, the 2014 Marie-Victorin Prize (Prix du Quebec), the 2015 Prix d'Excellence en Recherche et Innovation of Polytechnique Montréal, the 2015 IEEE Montreal Section Gold Medal of Achievement, the 2019 IEEE MTT-S Microwave Prize, the 2021 EIC Julian C. Smith Medal, the 2022 IEEE MTT-S Outstanding Educator Award, and the 2022 IEEE AP-S John Kraus Antenna Award. He has held key positions in and has served on various panels and international committees, including the Chair of technical program committees, international steering committees, and international conferences/symposia. In particular, he was the General Chair of the 2012 IEEE Microwave Theory and Techniques (IEEE MTT-S) International Microwave Symposium and the TPC Co-Chair of the 2020 IEEE International Symposium on Antennas and Propagation. He has served on the editorial/review boards for many technical journals, transactions, proceedings, and letters as well as scientific encyclopedia, including editor, track editor, and guest editor. He was the Chair of the joint IEEE Montreal chapters of MTT-S/AP-S/LEOS and then the restructured IEEE MTT-S Montreal Chapter, Canada. He has served the IEEE MTT-S and Administrative Committee (AdCom) as the Chair for the IEEE MTT-S Transnational Committee, the Member and Geographic Activities Committee, Technical Coordinating Committee, and the 2016 IEEE MTT-S President among many other AdCom functions. He is currently the Chair of the IEEE MTT-S Inter-Society Committee. He was a Distinguished Microwave Lecturer of the IEEE MTT-S from 2009 to 2011. He served the European Microwave Association as the Inaugural Representative of North America in its General Assembly. He is a Fellow of the Canadian Academy of Engineering, the Academy of Science of the Royal Society of Canada, and the German National Academy of Science and Engineering. He is a member of the Electromagnetics Academy, URSI, and IEEE-Eta Kappa Nu (IEEE-HKN).